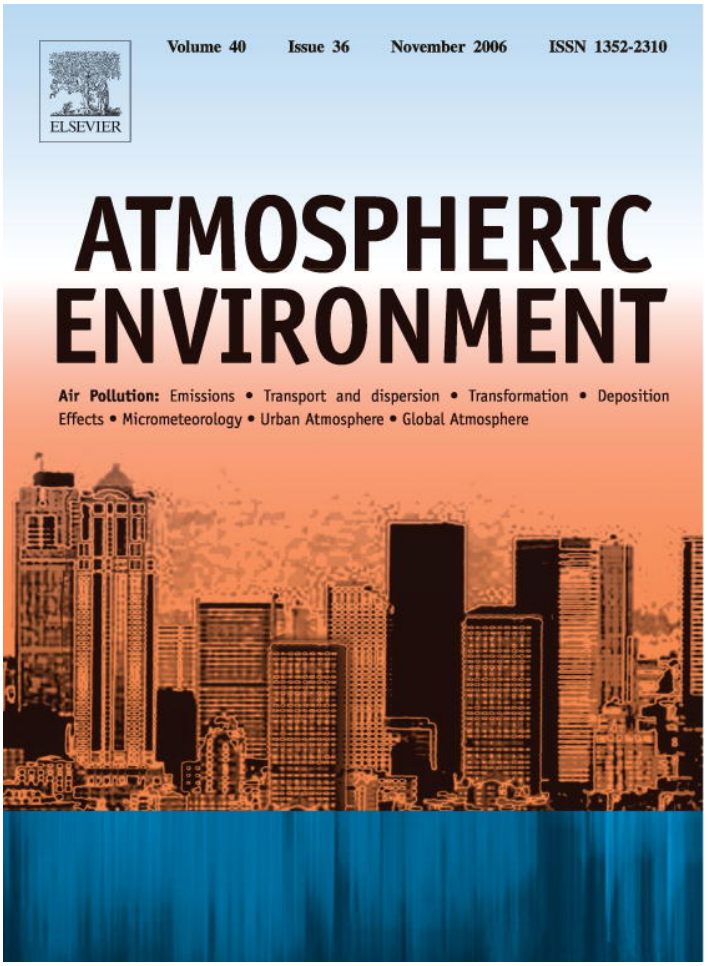

Available online at www.sciencedirect.com
ScienceDirect
Atmospheric Environment 40 (2006) 6975–6987
ATMOSPHERIC ENVIRONMENT
www.elsevier.com/locate/atmosenv

GOME aerosol optical depth retrieval over ocean: Correcting for the effects of residual cloud contamination

Elisa Carboni*

Clarendon Laboratory, Department of Physics, Atmospheric, Oceanic and Planetary Physics, University of Oxford, Parks Road, Oxford OX1 3PU, UK

Received 10 February 2006; received in revised form 9 June 2006; accepted 14 June 2006

Abstract

Aerosol optical depths (AODs) retrieved from GOME reflectances using a clear sky algorithm have been compared to AODs from ground-based sunphotometers. A systematic overestimation of GOME AOD was found, mainly due to the presence of clouds within the GOME field-of-view. In order to take the influence of clouds into account, a model which assumes a linear dependence of AOD on cloud fraction has been tested. This model was validated using independent measurements from different AERONET sites. The monthly averaged maps of corrected AOD show similar spatial behaviour to AVHRR and TOMS maps. The method proposed here produces monthly maps of AOD from GOME data. It is applicable on a statistical analysis (monthly) and is proved to be effective in regions with high AOD, but relatively large uncertainties remain for background marine conditions.

Keywords: Aerosol optical depth; Remote sensing; GOME data; AERONET sunphotometer; Earth observation

1. Introduction

Atmospheric aerosols influence the Earth's radiation balance by scattering and absorbing solar radiation (direct effect), and by modifying the micro-physical properties of clouds (indirect effect). The radiative forcing of direct and indirect aerosol effects is one of the largest uncertainties remaining in climate study (IPCC, 2001). Moreover, aerosol has high spatial and temporal variability. To better understand and reduce the uncertainties due to aerosol we need to study aerosol optical properties, aerosol loading and variability over the globe. Such information has to come from different instruments, with complementary observational capabilities, covering all relevant spatial and temporal time-scales.

Satellite remote sensing is able to provide continuous global observations of aerosol over multi-annual, even decadal times-scales. The Global Ozone Monitoring Experiment (GOME) is a nadir viewing grating spectrometer (Burrows et al., 1999) which made global observations between June 1995 and June 2003. The contiguously observed spectral range is 235–793 nm, which provides information in both the UV and the visible/near-ir. However, for the purposes of aerosol retrieval, a major limitation of the GOME instrument is its relatively large field-of-view (or *ground pixel*) of 40 × 320 km which is

*Tel.: +44 1865 272 915; fax: +44 1865 272 923.
E-mail address: elisa@atm.ox.ac.uk.

1352-2310/$ - see front matter © 2006 Elsevier Ltd. All rights reserved.
doi:10.1016/j.atmosenv.2006.06.035

scanned across a 960 km swath (in the standard observing mode). With this observing mode, global coverage is achieved within 3 days, but a very large fraction of the scenes are contaminated by cloud.

The goal of this paper is to develop a method to produce monthly maps of aerosol optical depth (AOD) over the sea starting from level-1 GOME data, that could be useful for climate studies. Satellite aerosol retrieval requires a very careful separation of the aerosol signal from measure ment uncertainties associated with radiometric calibration errors, inaccurate assumptions in the retrieval algorithm, atmospheric gas absorption, surface reflectance effects and cloud contamination. In particular the presence of cloud within the field-of-view is recognized as one of the major error sources in aerosol retrievals (Myhre et al., 2004; Zhao et al., 2003).

In the present work the AOD retrieval algorithm, based on that of Guzzi et al. (2001) and Torricella et al. (1999), is briefly summarised, focusing on differences with respect to the earlier work. The algorithm assumes scenes to be cloud-free but is nevertheless applied to scenes with up to 20% cloud fraction (only a small fraction of GOME scenes are truly cloud-free). Comparisons to Aeronet ground-based sun-photometer data (Holben et al., 1998) show that the scheme frequently overestimates the AOD due signal cloud contamination. To correct this error we test the hypothesis that this GOME AOD could be considered as a linear function of "clear AOD" (that is AOD if there was not cloud in the pixel) and an empirically scaled cloud fraction. This hypothesis is tested using AERONET measurements. Finally we compare monthly corrected AOD maps with other satellite data set available.

2. The influence of low cloud fraction on the AOD retrieval

To analyse GOME spectra we have used an atmospheric model that takes into account only the contribution of a clear-sky atmosphere over a dark surface, without considering any cloud. Any variation of the signal due to cloud presence can produce a systematic variation in the output of the AOD retrieval.

2.1. Selection of scenes

The FRESCO algorithm gives the cloud top pressures and effective cloud coverage fractions, f, derived from GOME data in the oxygen A-band (758–775 nm). In Koelemeijer et al. (2001), the FRESCO method is described together with a sensitivity study and a validation using ATSR-2 data. In Koelemeijer et al. (2002), a comparison is made between cloud top pressures and effective cloud fractions of FRESCO and ISCCP on a monthly average basis. For the current analysis, pixels over the ocean (excluding sun-glint regions), with solar zenith angle $<70^\circ$ and a FRESCO cloud-fraction of less than 20% are selected. Pixels over the polar regions (latitudes beyond 70°) are excluded.

2.2. Aerosol clear sky retrieval algorithm

A radiative transfer model (RTM), DOWNSTREAM (Levoni et al., 2001) is used to simulate top of atmosphere (TOA) reflectance spectra for different aerosol types and amounts over the sea surface. The computed TOA reflectances at a set of selected wavelengths, $R_{\mathrm{mod}}(\lambda_{i=1,N})$, are compared to measured satellite reflectance, $R_{\mathrm{exp}}(\lambda_{i=1,N})$, taking into account the measurement errors, $\sigma_{\mathrm{exp}}(\lambda_{i=1,N})$. For GOME the following wavelengths are selected for which gaseous absorption is very weak (transmittance $>99.7\%$): 364, 373, 385, 394, 424, 754.4, 780 nm. For each of a set of aerosol classes, the aerosol amount is varied until the best fit is obtained between the measured and simulated spectra, i.e. the following cost function is minimised.

$$\chi^2(\tau_{\mathrm{G}}, \mathrm{class}) = \sum_{i=1}^{N} \left(\frac{R_{\mathrm{exp}}(\lambda_i) - R_{\mathrm{mod}}(\lambda_i, \tau_{\mathrm{G}}, \mathrm{class})}{\sigma_{\mathrm{exp}}(\lambda_i)} \right)^2, \quad (1)$$

where the fitted parameter τ_{G} is AOD at the reference wavelength of 500 nm for each aerosol class. Each class has specific and fixed spectrally dependent optical properties, namely single scattering albedo, phase function and extinction coefficient relative to the value at 500 nm. Specifying a value for τ_{G} defines the extinction coefficient at 500 nm and hence the complete set of spectral optical properties.

The retrieval identifies the aerosol class by selecting the one which gives the lowest value of χ^2 (after optimising τ_{G} for each class). The selected class and corresponding τ_{G} are the reported results of the retrieval.

The spectral optical properties are calculated from micro-physical properties (size distribution

and refractive index) assuming spherical particles (Mie theory) as described in Levoni et al. (1997). The selected aerosol classes are Maritime (Shettle and Fenn, 1979), Desert (D'Almeida et al., 1991), Maritime polluted (D'Almeida et al., 1991), Volcanic Ash (WMO, 1986) and Biomass Burning (Dubovik et al., 2002). The RTM needs other inputs like sea-water spectral reflectivity (considered as Lambertian surface), Rayleigh scattering model and vertical aerosol profile. All these quantities are set according to Torricella et al. (1999) and Guzzi et al. (2001).

2.3. Criteria for comparing ground-based and satellite-based data

AODs retrieved from satellites need to be continuously compared with other aerosol measurements coming from different satellites and validated with ground-based instruments such as sunphotometers, which provide generally more accurate and precise estimates of AOD. However, due to the large spatial and temporal variability of aerosol and the different sampling characteristics of ground based and satellite instruments, we need to take care that observations are of truly comparably locations and times. In this study we use AERONET (Holben et al., 1998) level 2 quality assured data for different island sites. These data have passed a stringent cloud screening procedure.

To minimise the error due to presence of land inside GOME ground pixels, we have selected sites over islands with area less than $18 \times 18\,km^2$. We have also selected GOME data, whose reflectance spectrum does not present any anomaly such as jumps or offsets.

By considering the GOME pixel dimensions ($320 \times 40\,km^2$), we can expect that AOD may vary significantly within a GOME field-of-view. The instrument integrates the signal over pixel area, and then satellite data inversion gives an averaged AOD. Moreover, GOME overpasses each site at a specific local solar time (every 3 days) which is not identical to the time of the sunphotometer observation.

Here we compare GOME AOD (10:30 local solar time) with Aeronet level 2 AODs which are averaged over the sun-lit day, provided the AERONET station is within the GOME field-of-view. It may be assumed that the temporal averaging of the very localised Aeronet measurement compensates to some extent the spatial averaging over the field-of-view of the instantaneous GOME AOD. We therefore expect a more meaningful comparison between the GOME AOD and the daily average AERONET AOD rather than the individual observation made closest in time. Anyway, we have compared the AERONET AOD measured closest in time to the GOME observation with the daily mean and find that for 90% of cases the discrepancies are less than 0.05 in AOD.

2.4. Comparison between GOME and AERONET AOD

At present we have reprocessed GOME data from 1997 to 1999, and have compared AERONET AODs with this new data. During this period we have a restricted number of AERONET stations which supply a limited number of useful coincidences for comparison. We have considered the following sites:

- Kaashidhoo (Indian Ocean) 04°57′N, 73°27′E, altitude 0 m.
- Nauru (Pacific Ocean) 00°31′S, 166°54′E, altitude: 7 m.
- Bermuda (Atlantic Ocean) 32°22′N 64°41′W, altitude 10 m.

These sites are very different in latitude and geographic position and can be considered representative of different areas over the ocean.

Fig. 1 summarises the comparison between the retrieved AOD (τ_G) and the AERONET data for these stations. Different symbols refer to different ranges of values of cloud fraction. In the plotted data, GOME AODs are systematically overestimated compared to AERONET. We can observe that the overestimation increases within increasing cloud fraction. Only data with cloud fraction less than 1% could be consistent with the ground data. However, the number of coincidences with cloud fraction less than 1% is very low over Bermuda, Kaashidhoo and Nauru islands, we have only three GOME pixels with such a low cloud fraction.

However, the comparison between GOME AOD and AERONET is subject to other sources of uncertainty:

- Spatial/temporal sampling errors as discussed in Section 2.3.
- Presence of a small proportion of land in the GOME pixel, the albedo of which is not modelled in the retrieval scheme.

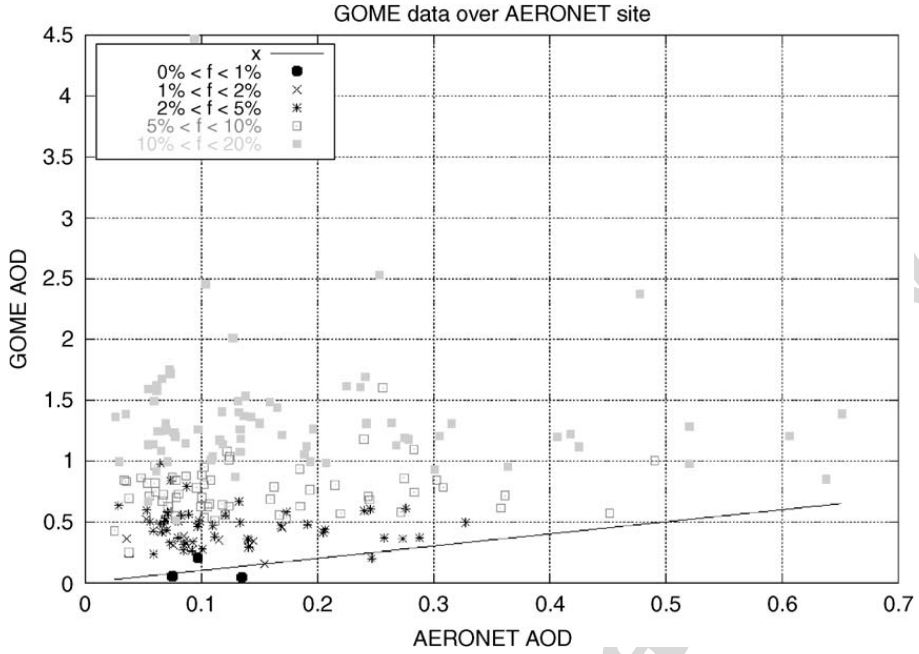

Fig. 1. GOME AOD retrieved with clear sky algorithm versus AERONET. The different symbols represent different cloud fractions. The GOME pixel cloud fraction is less than 20%. The line represents $y = x$; it is apparent that most of the data are plotted above this line, indicating that GOME AOD are systematically overestimated compared to AERONET. As cloud fraction increases, the discrepancy increases.

- Variability in ocean conditions such as sea roughness, pigment concentration and foam.
- Errors due to polarisation of light, mainly for clear pixels where the presence of molecules is prevalent.

However the major source of error is the presence of cloud in the field-of-view. The clear sky algorithm produces biased AODs data for cloud fraction $>1\%$.

3. Linear-clearing approach

With results from the clear sky algorithm applied to GOME scenes for one day (6 June 1997) with *any* cloud fraction, we examine the GOME AOD, τ_G, and aerosol class as function of the FRESCO effective cloud fraction.

As can be seen in Fig. 2, for cloud fraction $f > 50\%$ the GOME AOD (τ_G) is high (>5) and increases exponentially with cloud fraction. The algorithm selects the maritime class. This can be explained because maritime is (like cloud) a scattering class (single scattering albedo is greater than 0.97 for all the considered wavelengths). By increasing AOD the spectral reflectivity can increase and match the cloud reflectance at any single wavelength. However, the spectral shape due to cloud and maritime aerosol are different and the values of the resulted chi-squares become high (because a simultaneous match at all wavelengths is not possible). For $20\% < f < 50\%$ the GOME clear sky algorithm retrieves not only the maritime class but also sometimes maritime polluted, desertic and biomass burning. There is a significant number of pixels with a values of τ_G greater than 5, having an exponential trend with cloud fraction. For $f < 20\%$, τ_G shows a linear trend as function of f. In particular for $10\% < f < 20\%$ the aerosol class can be significantly retrieved when there is an aerosol event with high AOD. On the basis of this result, we have sought to correct the GOME AOD retrieved for $f < 20\%$ using a linear function of f.

3.1. Modelled TOA reflectance in the single scattering approximation

Considering the single scattering contribution to the satellite signal to be dominant, even if a small residual of clouds is present over the GOME ground pixel, the TOA reflectance over the dark ocean at reference wavelength, can be written as the sum of two contributions

$$R = R_m + R_{ac}, \quad (2)$$

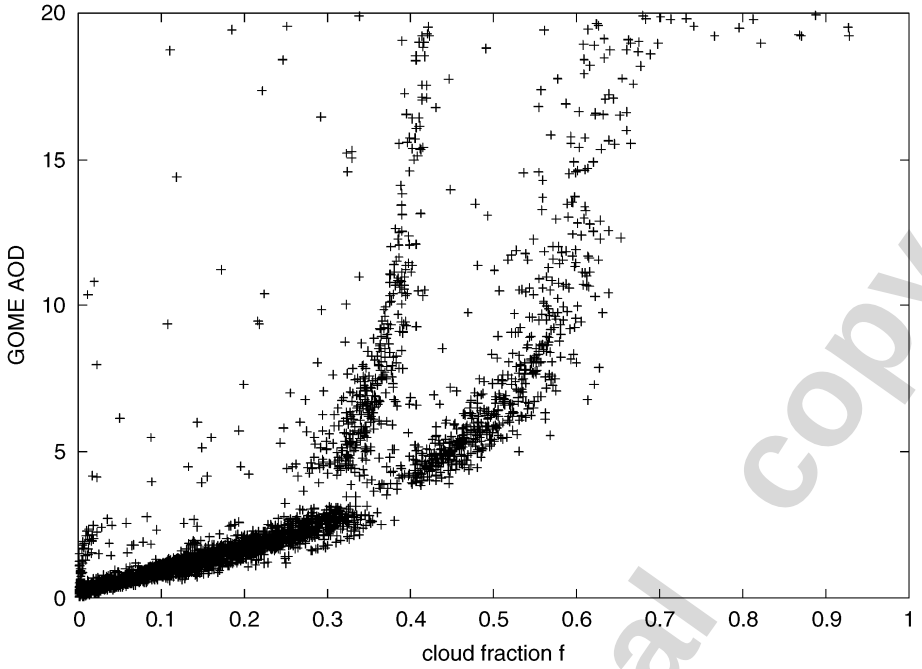

Fig. 2. GOME AOD values retrieved using the clear sky algorithm as function of FRESCO cloud fraction, f.

where R_m is the path reflectance due to molecular scattering and

$$R_{ac} = \frac{1}{4\mu\mu_0}\,\omega P(\mu,\mu_0,\Delta\phi)\tau_G \tag{3}$$

is the path reflectance due to the aerosol and residual cloud presence over ground pixel.

In Eq. (3) τ_G is the AOD retrieved by the clear sky Algorithm, as described in Section 2. Because of residual cloud in the scene, τ_G must be considered an *equivalent* AOD, while ω and $P(\mu,\mu_0,\Delta\phi)$ are the single scattering albedo and the phase function at 500 nm of the retrieved aerosol class, respectively. μ and μ_0 are the cosine of the viewing and solar zenith angle, respectively, and $\Delta\phi$ is the difference between the solar and viewing azimuth angle.

In Eq. (2) we ignore the contribution towards the satellite due to ocean surface, though this is included in the retrieval scheme.

Using the cloud coverage fraction f, the TOA reflectance R can also be written

$$R = fR_{m,c} + (1-f)R_{m,a}, \tag{4}$$

where $R_{m,c}$ is the TOA reflectance due to the fraction of the field-of-view covered by cloud (f) and $R_{m,a}$ is the contribution due to cloud-free fraction $(1-f)$.

In particular we consider

$$R_{m,c} = R_m + R_c. \tag{5}$$

Assuming single scattering

$$R_{m,a} = R_m + \frac{1}{4\mu\mu_0}\,\omega_a P_a(\mu,\mu_0,\Delta\phi)\tau_a \tag{6}$$

Eq. (2) is similar to Eq. (6), but in the latter the factors ω_a, P_a, and τ_a are, respectively, the single scattering albedo, the phase function, and the optical depth of the aerosol only. As indicated in Eq. (4), $fR_{m,c}$ is the contribution to the signal due to the fraction of pixel with clouds.

The comparison between Eqs. (2) and (4) leads to the following linear relation:

$$\tau_G = (1-f)\frac{\omega_a P_a}{\omega P}\,\tau_a + 4\mu\mu_0\,\frac{R_c}{\omega P} f \tag{7}$$

which links the "clear AOD" τ_a and the equivalent AOD τ_G to the cloud coverage fraction f.

As already mentioned, Eq. (7) is assumed valid for small values of f. Moreover, in this case, we also suppose the aerosol class employed in the aerosol retrieval is well representative of real aerosol type. This means that the approximation $\omega P \simeq \omega_a P_a$ can be considered valid. In particular, this is true on average for a large number of events. (We expect

that for a single event the value $\omega_a P_a$ can differ significantly from the aerosol database value.)

In that context Eq. (7) can be written in the following equivalent way:

$$\tau_G = (1-f)\tau_a + \alpha f, \tag{8}$$

where

$$\alpha = 4\mu\mu_0 \frac{(R_c)}{\omega P}. \tag{9}$$

In single scattering approximation we have determined the linear equation (8) between the retrieved AOD τ_G and the "clear AOD" τ_a. Eq. (8) shows that τ_G is a linear function of τ_a with a factor $(1-f)$; this factor represents the pixel's area fraction without clouds. When cloud fraction is equal to zero, τ_G is equal to τ_a. The retrieved AOD τ_G is a function of τ_a, of cloud fraction f and of a parameter α, which is related to the geometric conditions, to the aerosol optical properties and to the cloud reflectance at the wavelength considered.

In next section we investigate the possibility to apply the linear equation (8), found in single scattering approximation, for real data, including conditions where multiple scattering may be significant. We therefore now consider α as an empirical parameter found after using ground sunphotometer measurements, which have coincidences with GOME measurements for $f<20\%$.

3.2. Derivation of scaling parameter α

We consider as the best estimation of "clear AOD" τ_a the level 2.0 data of AERONET AOD. To test the linear relation of Eq. (8) we can use the coincidences between GOME and AERONET sites and look at the trend of $\tau_G - (1-f)\tau_a$ vs. f.

We choose to split the set of coincidences, within the years 1997–1999, into two groups of ground measurements. We use as the first group the measurements from the Bermuda site (85 coincidences), and as second group those from Kaashidhoo (65 coincidences). The first group is used to test the linear trend and estimate α. The second group is used to scale GOME AODs τ_G by inverting Eq. (8) and validate the obtained "clear GOME AODs" τ_a by comparison to the AERONET values (see Section 4.1).

Fig. 3 shows as a histogram, $\tau_G - (1-f)\tau_a$, binned by cloud-fraction in intervals of $\Delta f = 0.02$ (indicated by the horizontal bars). Vertical error bars are the RMS deviation within each bin.

According to Eq. (8) the data points should be fitted by a straight line passing through the origin, with the slope equal to the empirical factor α. Fitting such a line to the data (the solid line in the figure) gives $\alpha = 7.71 \pm 0.24$. A linear fit to the data which is not constrained to pass through the origin, $y = af + b$ (the dotted line of Fig. 3) yields a $\chi^2/n\,df = 11.9/8$, while the fit with αf gives a

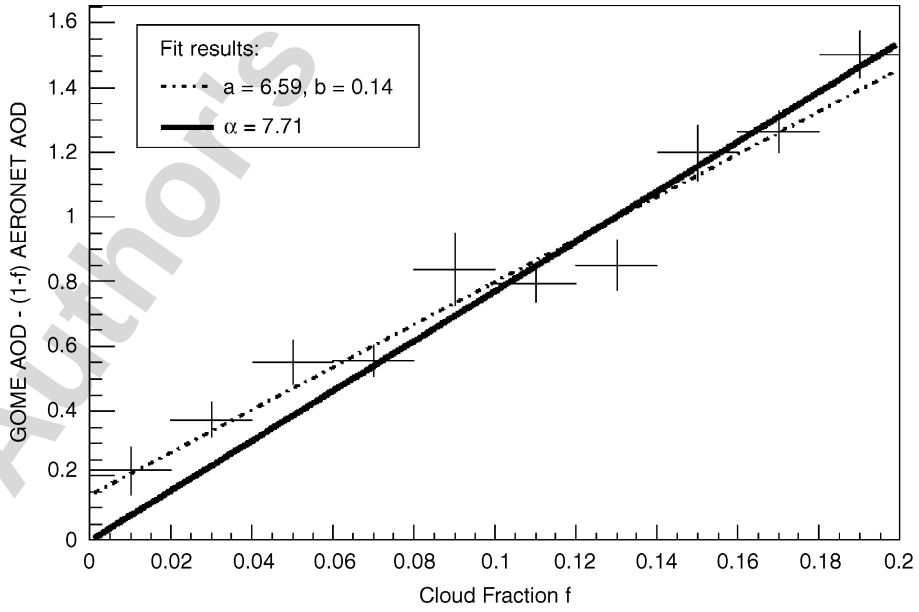

Fig. 3. Difference between GOME AOD and $(1-f)$ AERONET AOD vs. cloud fraction f at the Bermuda site. The dashed line corresponds to a linear fit by means of a first order polynomial $af + b$, while the solid black line is related to the proportional trend αf. The first fit yields a $\chi^2/n\,df = 11.9/8$, while the second one yields $\chi^2/n\,df = 23.8/9$.

somewhat larger $\chi^2/n\,\mathrm{d}f = 23.8/9$. However here we take the fit which passes through the origin, which is consistent with our model.

The same fit performed for Kaashidhoo data gives the value $\alpha = 7.62 \pm 0.33$, which is consistent with the value for Bermuda. For Nauru site we obtain $\alpha = 9.04 \pm 0.23$. This higher value may be due to a frequent overestimation of GOME AODs over Nauru site, as shown in the following section.

The linear trend could depend on the aerosol class. However, for this analysis we have a restricted number of AERONET coincidences, which does not allow us to distinguish between different classes. Similarly α may depend on cloud type.

By means of this procedure we therefore find an averaged coefficient α. It can be considered well representative for different oceanic locations, and we use it in all the processed GOME pixels. In particular, we test if α can be considered as the same as for different locations over the ocean as well as for different AERONET islands sites.

We scale GOME AODs at Kaashidhoo and Nauru site using the value of α estimated using Bermuda data. From Eq. (8)

$$\tau_a = \frac{\tau_G - \alpha f}{(1-f)}, \tag{10}$$

where τ_a is the corrected AOD. We compare these AOD values with the corresponding Kaashidhoo and Nauru values. The results are shown and discussed in the next section.

4. Results and discussion

4.1. Validation

The clearing method is tested by comparing satellite AOD data with AERONET AOD. Fig. 4, shows the scatter-plot of AERONET AOD and GOME AOD τ_a at the Kaashidhoo site, computed using the Bermuda α coefficient.

The straight line constrained to pass through the origin has a slope of 1.06 ± 0.13 (13%) with a standard deviation in AOD of 0.26.

We note that GOME AODs over Nauru site are generally overestimated compared to Nauru sun-photometer AODs. By comparing GOME scaled AOD maps with other instruments (see next section) we see that AODs are frequently overestimated over the East of Indonesia and Australia areas. This is probably due to the sea surface reflectance being higher than that considered in our model.

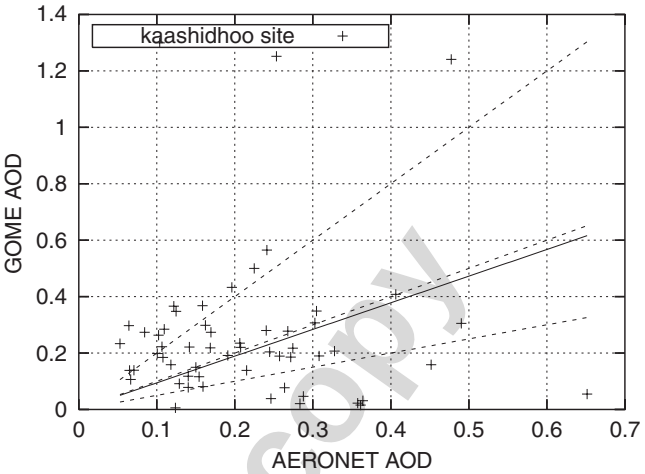

Fig. 4. Scatter plot for the Kaashidhoo site between AERONET AOD and GOME AOD. The solid line is obtained from linear regression with a line passing through the origin. The dotted lines are the ideal line with slope 2, 1 and $\frac{1}{2}$.

The slope of the straight line with or without Nauru data changes only a little: Without Nauru data the slope coefficient is 0.96 ± 0.16 (16%) with a standard deviation in AOD of 0.29.

We can note also that the furthest pixels from the line with slope equal to unity are for $f > 10\%$. Looking at a single measurement, we can significantly overunderestimate the retrieved AOD. By using the correction approach we remove most of the positive bias due to residual cloud in the GOME AODs retrieved with the clear sky algorithm. However, as noted previously there are other sources of error which can introduce more random differences in individual comparisons with AERONET data. In a statistical analysis, e.g. monthly average AOD, these differences may be smoothed to give a realistic averaged AOD. Results for monthly mean AOD are shown in the following section.

4.2. Comparison of global, monthly mean maps

Here, we compare the monthly average AOD from GOME data to other satellite instruments that give aerosol information over the ocean. In our comparison we use data from TOMS (Torres et al., 1998; Torres et al., 2002) and AVHRR (Mishchenko et al., 1999; Geogdzhayev et al., 2002).

The spatial resolution is very different and this could produce differences in maps, especially due to presence of clouds. In particular, GOME maps have more gaps due absence of data with $f < 20\%$.

To produce monthly average of GOME AODs we consider a global grid of $1^\circ \times 1^\circ$. When the coordinates of the central point of a single grid-box are inside a GOME field-of-view, the corresponding AOD is considered as a contribution to the monthly average value for this box. Moreover, to obtain global maps at different wavelength from 500 nm, we scale each AOD using the spectral extinction coefficients for the given aerosol class.

As an example, maps for April 1998 are shown in Fig. 5. Map (a) is the GOME aerosol maps obtained without the described cloud clearing procedure.

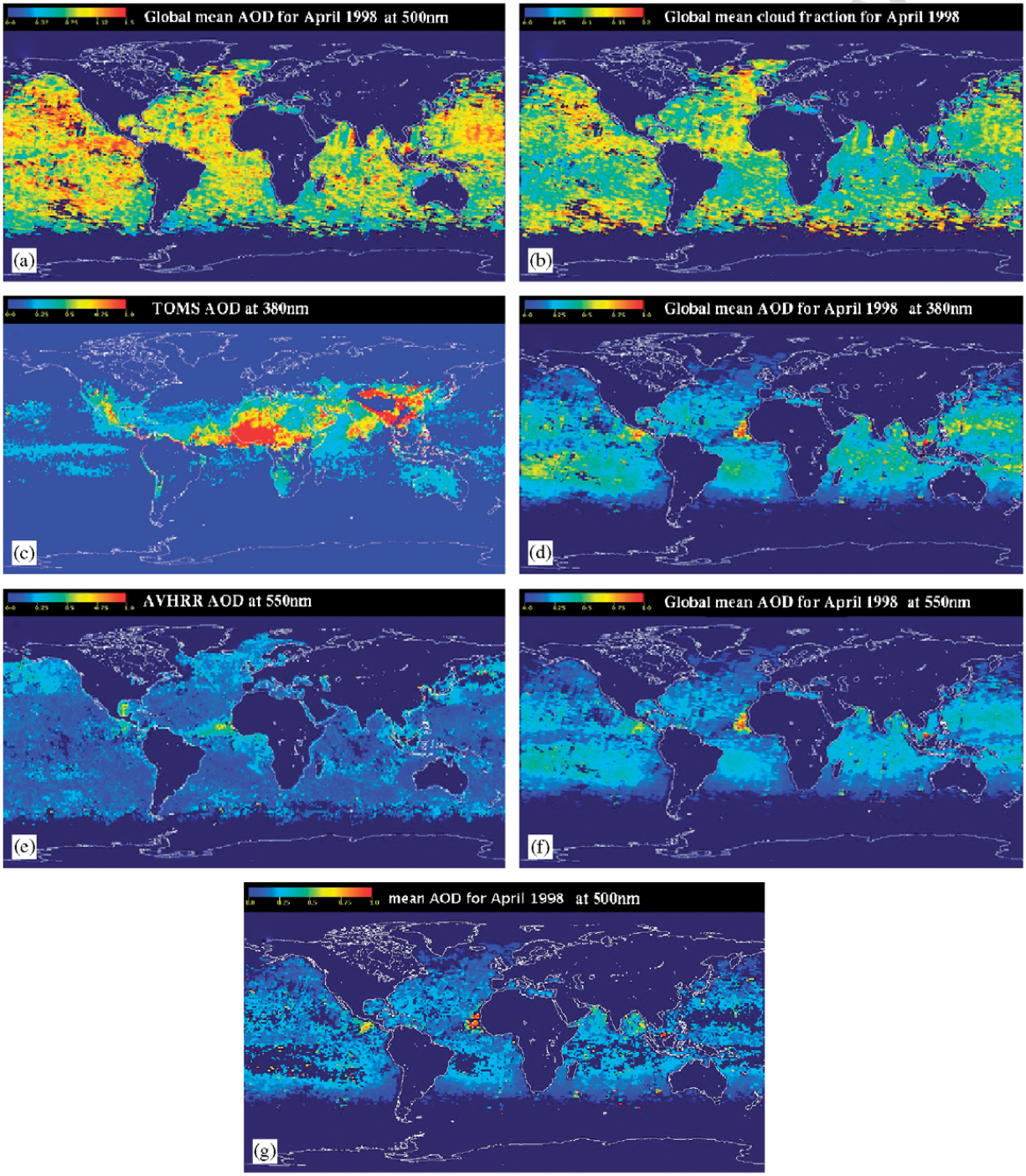

Fig. 5. Example of monthly average for April 1998: (a) aerosol optical depth at 500 nm from original GOME retrieval; (b) cloud fraction from FRESCO; (c) TOMS AOD; (d) GOME "clear AOD" scaled at 380 nm; (e) AVHRR (550 nm); (f) GOME "clear AOD" scaled at 550 nm and GOME "clear AOD" at 500 nm, respectively; and (g) GOME "clear AOD" at 500 nm, excluding some data as described in Section 4.2.

This figure has a colour scale from AOD 0–1.5 to clearly show the maximum values of AOD over the globe. We can observe that these maxima do not coincide with those seen by the other instruments.

Map (b) shows the mean cloud fraction used in our clearing procedure. Locations showing the maximum value of f are those which are affected most strongly by our correction procedure. This colour scale is between 0 and 0.2. All the other maps are shown with a colour scale from 0 to 1. Maps (c) and (d) show, respectively, TOMS AOD and GOME "clear AOD" scaled to 380 nm. Maps (e) and (f) show AVHRR and the GOME "clear AOD" as before but scaled to 550 nm.

In the corrected GOME data it is possible to discern aerosol features qualitatively similar to the other satellite data. From all instruments we can observe the high AOD due to fires in Central America, and the desert plume west of Africa. A high signal from Indonesia, which may be due to biomass burning, is present only in GOME data. A high AOD signal at west of India is present both in GOME and TOMS data.

There are some regions with high GOME AOD compared to other satellite data, like in the middle of Pacific oceans, west of South America and north-east of Indonesia. These systematically high values are probably due to some discrepancies of the spectral ocean reflectances compared to the modelled values: the spatial distribution of these high values shows some negative correlation with the phytoplankton distribution observed by POLDER.[1] At present there is a lack of literature on the behaviour of the ocean surface reflectance in the UV region (the GOME aerosol retrieval algorithm use four wavelengths below 400 nm). The high retrieved values are unlikely to be caused by remaining cloud contamination as the associated standard deviation in the monthly mean over these regions is very low.

Aerosol typically remains in atmosphere for a few days, high AOD and small variation over a whole month period are indicative of biased data. If, for example, we cut data with monthly average optical depth at 500 nm >0.3 and standard deviation <0.25 we obtain the AOD map shown Fig. 5(g). Note that the cut of persistently biased data removes the region that in (d) and (f) is overestimated compared to TOMS and AVHRR. The desert dust aerosol plume, to the west of Africa and the biomass burning events remain as they have relatively large standard deviation. A strategy to reprocess the data with a better model for the surface reflectance is under investigation.

4.3. Zonal mean AOD comparisons

Myhre et al. (2004) compare the monthly averaged AOD from different satellite measurements over the ocean, during the period from November 1996 to June 1997. During this period different satellite give the aerosol optical depth over ocean. These data were used in the Dedalus project.[2] Using this data it is possible—for the period January–June 1997—to compare GOME AOD with AVHRR, TOMS, OCTS and POLDER AODs. All data are rescaled at 550 nm.

For this study two different retrievals are available for AVHRR, a one-channel retrieval, AVHRR-1 (Stowe et al., 2002; Ignatov and Nalli, 2002), and a two-channel retrieval, AVHRR-2 (Geogdzhayev et al., 2002; Mishchenko et al., 1999). The TOMS (Torres et al., 1998; Torres et al., 2002) and AVHRR-2 data are available[3],[4] for the whole period 1997–1999. A description of the POLDER aerosol retrieval procedure is given in Goloub et al. (1999) and Deuze et al. (1999, 2000). The OCTS aerosol retrieval is described in Nakajima and Higurashi (1998), Higurashi and Nakajima (1999), and Higurashi et al. (2000).

Except for POLDER and OCTS, each instruments is on a different satellite with different orbit time. This issue could contribute to the differences between the data sets.

Fig. 6 shows the zonal average of monthly mean AOD over ocean obtained from the different instruments (POLDER, GOME, AVHRR1, AVH RR2, OCTS, TOMS) averaged for the first 6 months of 1997 (the common time-period for all data sets). The values are obtained, for every instrument, starting from monthly maps with $1^\circ \times 1^\circ$ box resolution, and taking the average of all the box at one latitude over in the 6 month period. The values are plotted only over the latitude range for which >10 GOME values exist. GOME zonal means are presented with and without the high mean/low standard-deviation cut described in the previous section. This cut mainly affects the region

[1] http://polder.cnes.fr/en/index.htm

[2] http://www-loa.univ-lille1.fr/Daedalus/index.htm

[3] AVHRR data: http://gacp.giss.nasa.gov/retrievals/

[4] TOMS data: http://toms.gsfc.nasa.gov/

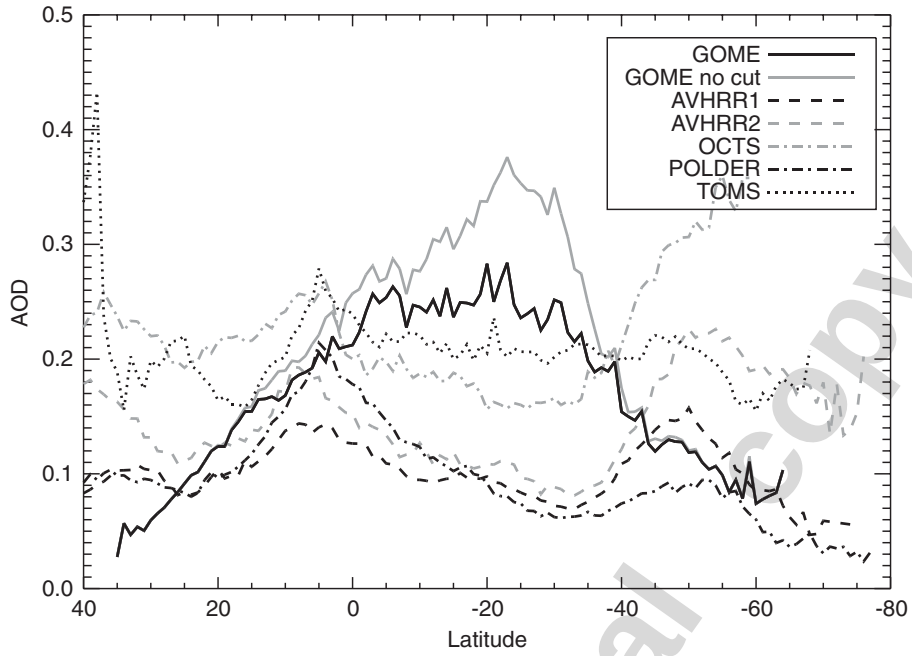

Fig. 6. Zonal average mean AOD obtained from the different instruments (POLDER, GOME, AVHRR1, AVHRR2, OCTS, TOMS). January–June 1997.

between 0 and -40° latitude but presents different patterns depending on month.

The large zonal differences between the retrievals over open ocean are striking. In particular the differences are large at midlatitudes in the Southern Hemisphere. The corresponding global mean AODs at 550 nm are the following: 0.20 (GOME), 0.11 (AVHRR-1), 0.14 (AVHRR-2), 0.21 (OCTS), 0.12 (POLDER), 0.22 (TOMS). The different instruments present considerable dispersion in zonal values and global mean. This means that also the background marine condition is significantly different from different instrument and algorithms (Myhre et al., 2004 suggests some of the difference may be due to cloud).

4.4. Case study: Capo Verde

Using the new corrected GOME data we can observe high and persistent aerosol events. An example of this is the Sahara desert dust plume, which periodically overpasses the ocean at west of Africa. In this region, at Capo Verde Island, there is an AERONET sunphotometer. We can compare data from different satellites (GOME, AVHRR and TOMS), and AERONET in the period 1997–1999. As said previously, the ground sunphotometer measures the columnar AOD corresponding to the vertical path over the station. On the other hand, the satellite measurements correspond to an average over an extended field-of-view. In our retrieval algorithm we reject pixels that exactly overpass Capo Verde Island, because the land fraction is too large for the retrieval scheme. We can make a comparison between this satellite monthly mean AOD and the monthly mean AERONET AOD at Capo Verde (16°43′N, 22°56′W, 60 m). The satellites have different spatial resolutions (GOME having by far the largest). At this latitude a GOME ground pixel typically covers three degrees of longitude. To obtain a comparable AOD from all satellite instruments we therefore consider the mean AOD over a region of $5^\circ \times 5^\circ$ around Capo Verde. The monthly mean of AERONET data is generated from the daily means of all available measurements.

Fig. 7(a) and (b) compare the AOD monthly averages at 380 nm of TOMS, AERONET and "clear" GOME AOD scaled to same reference wavelength. Fig. 7(c) and (d) show the AVHRR data at 550 nm, the "clear" GOME AOD and AERONET data, related to the same reference wavelength. These data are retrieved over the Capo Verde region during the years 1997 and 1999. At 380 nm the averaged difference between GOME and AERONET monthly AODs is -0.06 ± 0.03, while the averaged difference between TOMS and AERONET is 0.04 ± 0.03. Moreover, at 550 nm the averaged difference between GOME and AERONET is -0.11 ± 0.03 and the difference between AVHRR and AERONET is -0.14 ± 0.03. TOMS

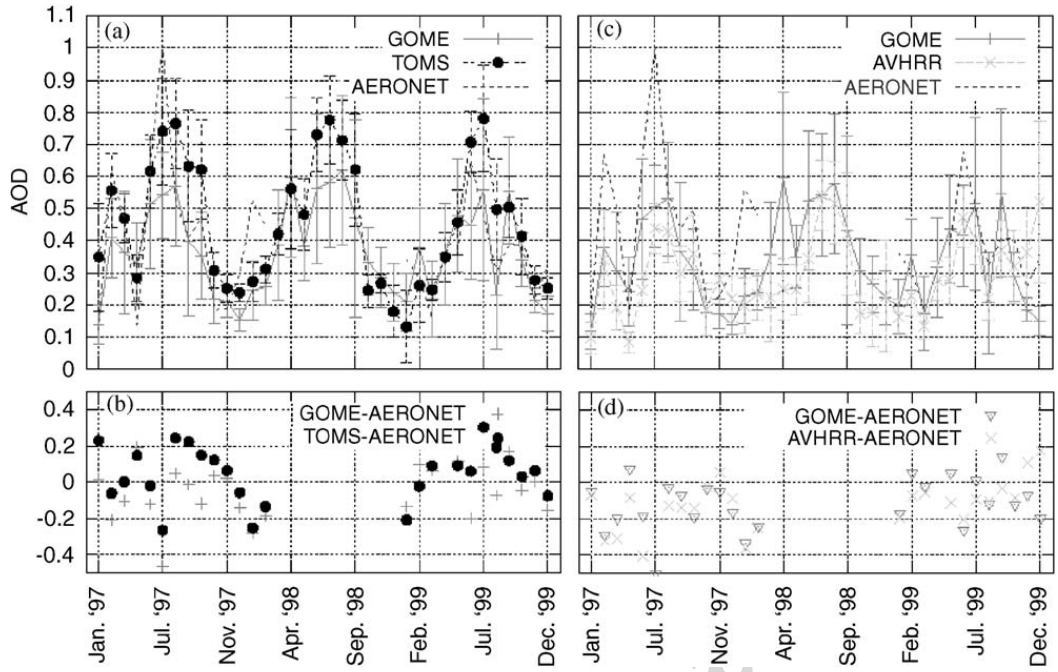

Fig. 7. (a) Monthly averages of AOD at 380 nm for the Capo Verde region from AERONET, TOMS and corrected GOME; (b) AOD (at 380 nm) differences between satellites and AERONET AOD; (c) monthly averages of AOD at 550 nm from AERONET, AVHRR and corrected GOME; (d) AOD (at 550 nm) differences between satellite and AERONET AOD. The satellite monthly regional average values refer to the $5^\circ \times 5^\circ$ oceanic region around Capo Verde.

averaged data overestimate the aeronet averaged AOD; AVHRR underestimates AERONET; GOME, which uses the combined spectral range of the two instruments, output data whose behaviour is between TOMS and AVHRR. However, all the analysed instruments present similar annual variation, with maximum AOD values between May and September.

5. Conclusion

Although the primary GOME objective is to determine the amount and distribution of atmospheric trace gases constituents its contiguous coverage allows uv-visible windows with negligible atmospheric absorption to be selected from which it is possible to retrieve aerosol information using a suitable algorithm.

The comparison between GOME and AERONET sunphotometer data is subject to different sources of uncertainties. However the major source of error in GOME retrievals using the previous clear sky algorithm is the presence of cloud in the field-of-view.

The clear sky algorithm is not able to retrieve AODs data comparable to AERONET AODs for cloud fraction $f > 0.01$. For small effective cloud fraction ($f < 0.2$) it is possible to use the linear equation $\tau_G = (1-f)\tau_a + \alpha f$ to determine the "clear AOD" τ_a, using an empirical parameter α found by comparison of τ_G with coincident AERONET data. This clearing procedure produces acceptable AOD retrievals.

The cloud correction presented in this work allows the retrieval of AODs which are consistent with other sensors both at the regional and global scales. However other retrieval problems still exist and future work is planned to address them: improvement of surface reflectance model, updates of aerosol models (in particular the imaginary part of the desert refractive index) and a study of α dependency on aerosol class.

The clearing procedure has so far been applied only to GOME data from 1997 to 1999. It is possible to extend the scheme to analyse the complete record starting in 1995 from GOME, Envisat-SCIAMACHY and, in future, by GOME-2 on Metop. This would yield a multi-decade data set which could be of significant value for climate studies.

Acknowledgements

Thanks to R. Guzzi, W. Di Nicolantonio, G. Ballista and ISAC-CNR institute for support,

suggestions and comments. This work would not have been possible without the various ground and satellite data. In particular we would like to acknowledge: B.N. Holben, D. Tanre', M.J. Bartholomew for AERONET data; M.I. Mishchenko and A. Ingatov for AVHRR data; O. Torres for TOMS data; J.L. Deuze for POLDER data; T. Nakajima for OCTS data.

References

Burrows, J.P., Weber, M., Buchwitz, M., Rozanov, V., Ladstatter-Weissenmayer, A., Richter, A., DeBeek, R., Hoogen, R., Bramstedt, K., Eichmann, K., Eisinger, M., 1999. The global ozone monitoring experiment (GOME): mission concept and first scientific results. Journal of the Atmospheric Sciences 56, 151–175.

D'Almeida, G.A., Koepke, P., Shettle, E.P., 1991. Atmospheric Aerosols. Global Climatology and Radiative Characteristics. Deepak, Hampton, VA.

Deuze, J.L., Herman, M., Goloub, P., Tanre, D., Marchand, A., 1999. Characterization of aerosols over ocean from POLDER/ADEOS-1. Geophysical Research Letters 26, 1421–1424.

Deuze, J.L., Goloub, P., Herman, M., Marchand, A., Perry, G., Susana, S., Tanre, D., 2000. Estimate of the aerosol properties over the ocean with POLDER. Journal of Geophysical Research 105, 15,329–15,346.

Dubovik, O., Holben, B., Eck, T.F., Smirnov, A., Kaufman, Y.J., King, M., Tanre, D., Slutsker, I., 2002. Variability of absorption and optical properties of key aerosol type observed in worldwide locations. Journal of Atmospheric Sciences 59, 590–608.

Geogdzhayev, I.V., Mishchenko, M.I., Rossow, W.B., Cairns, B., Lacis, A.A., 2002. Global two-channel AVHRR retrievals of aerosol properties of the ocean for the period of NOAA-9 observations and preliminary retrievals using NOAA-7 and NOAA-11 data. Journal of Atmospheric Sciences 59, 262–278.

Goloub, P., Tanre, D., Deuze, J.L., Herman, M., Marchand, A., Breon, F.M., 1999. Validation of the first algorithm applied for deriving the aerosol properties over the ocean using the POLDER ADEOS measurements. IEEE Transactions on Geoscience and Remote Sensing 37, 1586–1596.

Guzzi, R., Ballista, G., Di Nicolantonio, W., Carboni, E., 2001. Aerosol maps from GOME data. Atmospheric Environment 35, 5079–5091.

Higurashi, A., Nakajima, T., 1999. Development of a two-channel aerosol retrieval algorithm on a global scale using NOAA AVHRR. Journal of the Atmospheric Sciences 56, 924–941.

Higurashi, A., Nakajima, T., Holben, B.N., Smirnov, A., Frouin, R., Chatenet, B., 2000. A study of global aerosol optical climatology with twochannel AVHRR remote sensing. Journal of Climate 13, 2011–2027.

Holben, B.N., Eck, T.F., Slutsker, I., Tanre, D., Buis, J.B., Seltzer, A., Vermote, E., Reagan, J.A., Kaufman, J.A., Nakajima, T., Lavenu, F., Jankowiak, I., Smirnov, A., 1998. AERONET—a federated instrument network and data archive for aerosol characterization. Remote Sensing of Environment 66, 1–16.

Ignatov, A., Nalli, N., 2002. Aerosol retrievals from multiyear multisatellite AVHRR Pathfinder atmosphere (PATMOS) dataset for correcting remotely sensed sea surface temperatures. Journal of Atmospheric and Oceanic Technology 12, 1986–2008.

IPCC (Intergovernmental Panel on Climate Change), 2001. V. Ramaswamy, O. Boucher, J. Haigh, D. Hauglustaine, J. Haywood, G. Myhre, T. Nakajima, G.Y. Shi, S. Solomon, Radiative forcing of climate change. In: J.T. Houghton, et al. (Eds.), Climate Change 2001, The Scientific Basis, Contribution of Working Group I to the Third Assessment Report of the International Panel on Climate Change, Cambridge University Press, Cambridge, MA, pp. 349–416 (Chapter 6).

Koelemeijer, R.B., Stammes, A.P., Hovenier, J.W., de Haan, J.F., 2001. A fast method for retrieval of cloud parameters using oxygen A band measurements from the global ozone monitoring experiment. Journal of Geophysical Research 106, 3475–3490.

Koelemeijer, R.B., Stammes, A.P., Hovenier, J.W., de Haan, J.F., 2002. Global distributions of effective cloud fraction and cloud top pressure derived from oxygen A band spectra measured by the global ozone monitoring experiment: comparison to ISCCP data. Journal of Geophysical Research 107, doi:10.1029/2001JD000840.

Levoni, C., Cervino, M., Guzzi, R., Torricella, F., 1997. Atmospheric aerosol optical properties: a data base of radiative characteristics for different components and classes. Applied Optics 36 (30), 8031–8041.

Levoni, C., Cattani, E., Cervino, M., Guzzi, R., Di Nicolantonio, W., 2001. Effectiveness of the MS-method for computation of the intensity field reflected by a multi-layer plane-parallel atmosphere: results from an accelerated yet accurate radiative transfer code. Journal of Quantitative Spectroscopy and Radiative Transfer 69 (5), 635–650.

Mishchenko, M.I., Geogdzhayev, I.V., Cairns, B., Rossow, W.B., Lancis, A.A., 1999. Aerosol retrievals over the ocean by use of channels 1 and 2 AVHRR data: sensitivity analysis and preliminary results. Applied Optics 38 (36), 7325–7341.

Myhre, G., Stordal, F., Johnsrud, M., Ignatov, A., Mishchenko, M., Geogdzhaeyev, I., Tanre, D., Goloub, P., Nakajima, T., Higurashi, A., Torres, O., Holben, B., 2004. Intercomparison of satellite retrieved aerosol optical depth over ocean. Journal of Atmospheric Sciences 61 (5), 499–513.

Nakajima, T., Higurashi, A., 1998. A use of two-channel radiances for an aerosol characterization from space. Geophysical Research Letters 25, 3815–3818.

Shettle, E.P., Fenn, R.W., 1979. Models for aerosol lower atmosphere and effects of humidity variations on their optical properties, Report Tr-79-0214, U.S. Air Force Geophysics Laboratory, Hanscom Air Force Base, Massachusetts, 1979.

Stowe, L., Jacobowitz, H., Ohring, G., Knapp, K., Nalli, N., 2002. The AVHRR Pathfinder Atmosphere (PATMOS) climate data set: Initial analyses and evaluation. Journal of Climate 15, 1243–1260.

Torres, O., Bhartia, P.K., Herman, J.R., Ahmad, Z., 1998. Derivation of aerosol properties from satellite measurements of backscattered ultraviolet radiation. Theoretical basis. Journal of Geophysical Research 103, 17,099–17,110.

Torres, O., Bhartia, P.K., Herman, J.R., Sinyuk, A., Holben, B., 2002. A long term record of aerosol optical thickness from

TOMS observations and comparison to AERONET measurements. Journal of Atmospheric Sciences 59, 398–413.
Torricella, F., Cattani, E., Cervino, M., Guzzi, R., Levoni, C., 1999. Retrieval of aerosol properties over ocean using GOME measurements: methods and applications to test cases. Journal of Geophysical Research 104, 12,085–12,098.
World Meteorological Organization: A preliminary cloudless standard atmosphere for radiation computation. WCP-112 (World Climate Research Program, CAS, Radiation Commission of IAMAP, Boulder, Colorado, 1986).
Zhao, T.X.-P., Laszlo, I., Holben, B.N., Pietras, C., Voss, K.J., 2003. Validation of two-channel VIRS retrievals of aerosol optical thickness over ocean and quantitative evaluation of the impact from potential subpixel contamination and surface wind effect. Journal of Geophysical Research 108 (D3) 4106, doi:10.1029/2002JD002346.